PAPER • **OPEN ACCESS**

Silk fibroin increases the elasticity of alginate-gelatin hydrogels and regulates cardiac cell contractile function in cardiac bioinks

To cite this article: L Vettori *et al* 2024 *Biofabrication* **16** 035025

Biofabrication

PAPER

Silk fibroin increases the elasticity of alginate-gelatin hydrogels and regulates cardiac cell contractile function in cardiac bioinks

L Vettori[1,6], H A Tran[2], H Mahmodi[1], E C Filipe[4,5], K Wyllie[4,5], C Liu Chung Ming[1,6], T R Cox[4,5], J Tipper[1,7], I V Kabakova[1], J Rnjak-Kovacina[2] and C Gentile[1,3,6,*]

[1] University of Technology Sydney, Ultimo, NSW 2007, Australia
[2] University of New South Wales, Kensington, NSW 2052, Australia
[3] University of Sydney, Camperdown, NSW 2050, Australia
[4] The Garvan Institute of Medical Research and The Kinghorn Cancer Centre, Darlinghurst, NSW 2010, Australia
[5] School of Clinical Medicine, St Vincent's Healthcare Clinical Campus, UNSW Medicine and Health, Sydney, NSW 2052, Australia
[6] The Heart Research Institute, Newtown, NSW 2042, Australia
[7] Royal Melbourne Institute of Technology, Melbourne, VIC 3000, Australia
* Author to whom any correspondence should be addressed.

E-mail: Carmine.Gentile@uts.edu.au

Keywords: silk fibroin, bioink, alginate, gelatin, hydrogels, cardiac spheroids, bioprinting

Supplementary material for this article is available online

OPEN ACCESS

RECEIVED
12 October 2023

REVISED
11 March 2024

ACCEPTED FOR PUBLICATION
22 May 2024

PUBLISHED
4 June 2024

Abstract

Silk fibroin (SF) is a natural protein extracted from *Bombyx mori* silkworm thread. From its common use in the textile industry, it emerged as a biomaterial with promising biochemical and mechanical properties for applications in the field of tissue engineering and regenerative medicine. In this study, we evaluate for the first time the effects of SF on cardiac bioink formulations containing cardiac spheroids (CSs). First, we evaluate if the SF addition plays a role in the structural and elastic properties of hydrogels containing alginate (Alg) and gelatin (Gel). Then, we test the printability and durability of bioprinted SF-containing hydrogels. Finally, we evaluate whether the addition of SF controls cell viability and function of CSs in Alg–Gel hydrogels. Our findings show that the addition of 1% (w/v) SF to Alg–Gel hydrogels makes them more elastic without affecting cell viability. However, fractional shortening (FS%) of CSs in SF–Alg–Gel hydrogels increases without affecting their contraction frequency, suggesting an improvement in contractile function in the 3D cultures. Altogether, our findings support a promising pathway to bioengineer bioinks containing SF for cardiac applications, with the ability to control mechanical and cellular features in cardiac bioinks.

1. Introduction

Cardiovascular disease, including heart attack and heart failure (HF), is the leading cause of death worldwide [1]. Following the irreversible damage caused by a heart attack (or 'myocardial infarction'), healthy cardiomyocytes die and are replaced by fibrotic tissue that develops into a failing heart [2]. Given the limited availability of heart transplants and the risks associated, such as rejection, vasculopathies and infections, leading to poor survival of patients, novel strategies for HF patients are needed. In this regard, tissue engineering applied to regenerative medicine presents the promises to facilitate the replacement of the fibrotic heart with viable and functional bioengineered cardiac tissue from patient-derived cells [2, 3]. To better address the clinical need for personalised tissues, our team has previously developed iPSCs-derived cardiac spheroids (CSs), which better mimic the cardiac microenvironment for *in vitro* and *in vivo* applications [3, 4]. These present a complete endothelial cell network that prevents hypoxia and associated necrosis, while facilitates biofabrication of complex tissue with diverse morphology [3–5]. Given their ability to act as building blocks in permissive alginate (Alg)–gelatin (Gel) hydrogels, they have been explored for cardiac bioprinting, showing promising effects on the improvement of cardiac function when transplanted *in vivo* [4].

Alg enables the extrusion of the bioink that can then be cross-linked ionically with calcium chloride, while Gel promotes bioactivity in inert Alg hydrogels [6, 7]. Their combination in cardiac bioinks has shown high biocompatibility, while maintaining high viability and function of 3D CSs [3, 5]. Nevertheless, they present soft mechanical properties that may limit their use for *in vivo* applications in humans [5]. For instance, they tend to degrade in physiological environments (37 °C, 5%CO_2 in cell culture medium) [8].

Silk is a strong and stable polymer that has been extensively explored for vascular applications and has emerged as a promising biomaterial for cardiac tissue engineering applications [9–13]. SF is a natural protein produced by the *Bombyx mori* silkworm [1, 14]. SF fibers present non-repetitive hydrophilic α-motifs (light chains) and repetitive hydrophobic β-sheets (heavy chains), which confer respectively elasticity and strength to the fiber [1, 15]. In its regenerated form, SF molecules interact through non-covalent bonds such as hydrogen bonding, between the α-helices and β-sheets (as reported in supplementary figure 1) [1, 16]. Alternatively, SF can be added to other formulations to have better control over their mechanical properties and degradation rates [17, 18], which can create new hydrogen bonding and electrostatic interactions. For instance, sodium Alg and SF blend through intermolecular hydrogen bonds, which occur between the carboxyl group (COO–) of Alg and the amide group of SF (–NH_2), the amide group (both the C=O and –NH_2) of SF and –OH molecules in Alg polymer. Sodium Alg also binds with Gel through intermolecular hydrogen bonds between its –OH molecules and the carboxyl (COOH) and amide group (NH_2) of Gel. Gel and SF create electrostatic interactions, for instance between the carboxyl group (COOH) of SF and the amide group (NH_2) of Gel, as well as between the –OH group of SF and the carboxyl group (COOH) of Gel (supplementary figure 1) [19, 20].

Because of silk hydrophilic motifs, SF-containing hydrogels are used to increase hydration and porosity to support cell viability, migration, nutrient diffusion and oxygen delivery [1, 14, 21]. Given the tuneable properties of SF and its low immunogenic response in the human body, SF has shown great potential to be used as biomaterial for cardiac bioink formulations and cardiac tissue engineering applications [1, 22]. However, SF solutions cannot be printed by itself or without any further modifications (e.g. through its methacrylation [23]). This is due to its slow gelation rates and β-sheets formation, preventing its extrusion through a nozzle [1].

In this study, we investigated for the first time whether the addition of SF to Alg–Gel hydrogels could control their mechanical properties and their effects on cell viability and function. Our hypothesis is that the addition of silk fibroin (SF) to Alg–Gel hydrogels may regulate their elasticity without affecting cardiac cell viability *in vitro* and may improve cardiac function *in vivo*. This was tested by combining different concentrations of SF with 4% (w/v) Alg-8% (w/v) Gel hydrogels to evaluate any effects on hydrogel properties and cardiac cell viability and function. First, we evaluated the impact of 1% and 2% SF-containing hydrogels on hybrid hydrogel microstructure using scanning electron microscopy (SEM), and then on mechanical properties via classic compression and rheology testing, as well as advanced and non-destructive Brillouin spectroscopy. Brillouin spectroscopy is highly sensitive to changes in microscopic elasticity and viscosity [24–26]. Then, we analyzed the printability and durability of bioprinted SF-containing hydrogels in cell culture medium at 37 °C. Finally, SF–Alg–Gel hydrogels were tested for their use as bioinks to encapsulate CSs (figure 1).

Even though previous studies focused on the development of advanced 3D devices and/or platforms for tissue engineering as well as 3D cell constructs in different kinds of applications, this is the first one to investigate whether SF increases the elasticity of alginate–gelatin hydrogels and regulates cardiac cell contractile function in cardiac bioinks. For instance, Guarino *et al* [27] investigated the role of scaffolds and hydrogels in osteochondral and intervertebral disc tissue engineering. They concluded that the use of composite and/or hybrid hydrogels made by combining both natural- and synthetic-based polymers or adding synthetic peptides is promising for the design of 3D structures with improved mechanical properties, as well as enhanced swelling and degradation rates. Additionally, Reitmaier *et al* [28], studied the biomechanical features of a nucleus disc 3D model. In particular, they investigated whether the alterations in the mechanical properties of the model were affecting the functionality and the biomechanical behaviour after implantation in the native environment. Here, we demonstrate that the addition of SF to Alg–Gel hydrogels improves their durability in cell culture medium, as well as it increases the elasticity of the bioprinted patches. Our study also showed that the addition of SF-containing hydrogels improves the contractile activity of CSs compared to when they are embedded in Alg–Gel hydrogels alone. Altogether, our findings suggest that SF-containing hydrogels can be used to control mechanical and cellular features in bioprinted cardiac patches, with the potential to be used for cardiac applications. This will help to better control the elasticity of hydrogels that include other polymers than alginate-gelatin for advanced bioprinting techniques.

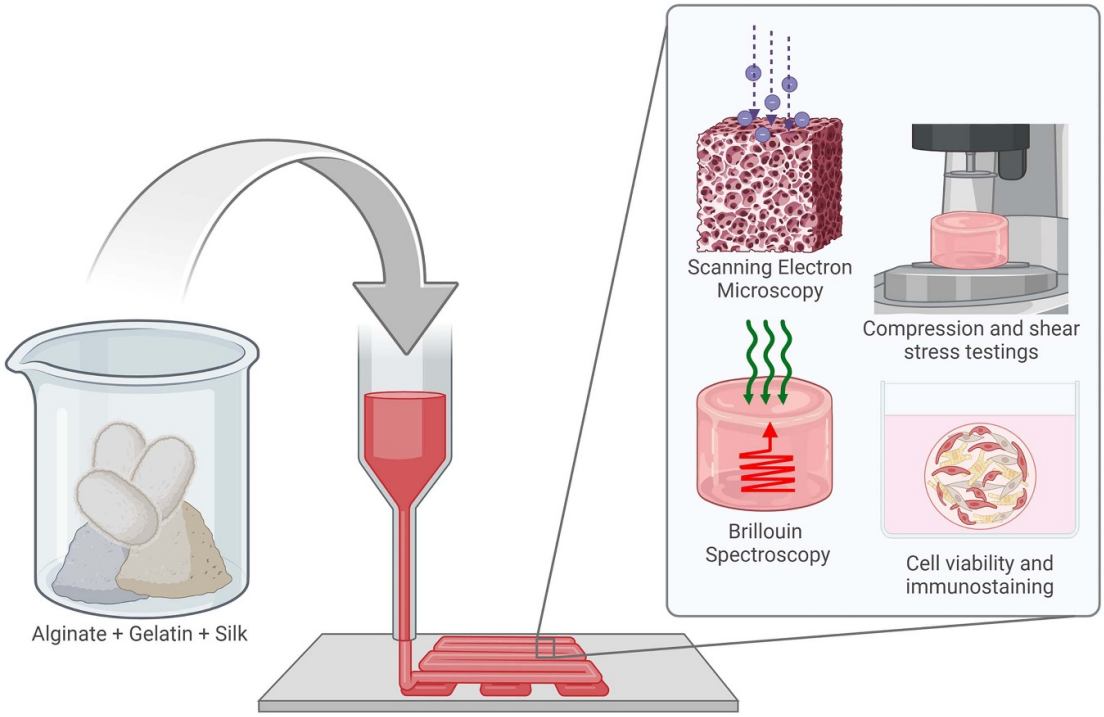

Figure 1. Schematic representation of alginate–gelatin–silk fibroin hydrogels preparation and characterization silk fibroin is mixed with alginate and gelatin natural-based polymers to biofabricate a hybrid hydrogel formulation. This hydrogel formulation is 3D bioprinted, in order to analyse its microstructure by SEM, mechanical properties by compression testing and Brillouin microscopy, cell viability and function with cardiac cells.

2. Material and methods

For SF extraction, sodium carbonate (Sigma-Aldrich, Darmstadt, Germany) and lithium bromide (Sigma-Aldrich, Darmstadt, Germany) were used. For hydrogels preparation, sodium alginate (Sigma-Aldrich, Darmstadt, Germany) and gelatin from bovine skin (Sigma-Aldrich, Darmstadt, Germany) powders were dissolved in Dulbecco Modified Eagle's Medium-high glucose medium (Sigma-Aldrich, Darmstadt, Germany) containing 50 units ml^{-1} penicillin and 50 μg streptomycin ml^{-1} (Gibco, ThermoFisher Scientific, Waltham, MA, USA) and 200 mM L-glutamine (Gibco, ThermoFisher Scientific, Waltham, MA, USA). To crosslink Alg–Gel–SF hybrid hydrogels, calcium chloride (Sigma-Aldrich, Darmstadt, Germany) was dissolved in Dulbecco's phosphate buffered saline (Sigma-Aldrich, Darmstadt, Germany).

For 2D cell culture, human coronary artery endothelial cells (Cell Applications, Inc., San Diego, CA, USA) were cultured in MesoEndo Cell Growth Medium (Cell Applications, Inc., San Diego, CA, USA), while human cardiac fibroblasts (CFs) (Cell Applications, Inc., San Diego, CA, USA) were cultured in CFs Growth Medium (Cell Applications, Inc., San Diego, CA, USA). Human induced pluripotent stem cell-derived cardiomyocytes[2] (Fujifilm Cellular Dynamics, Inc., Madison, Wisconsin, USA) were cultured on fibronectin (bovine, Sigma-Aldrich, Darmstadt, Germany) pre-coated flasks using iCell Cardiomyocytes Plating Medium (Fujifilm Cellular Dynamics, Inc., Madison, Wisconsin, USA). Plating Medium was replaced with iCell Cardiomyocytes Maintenance Medium (Fujifilm Cellular Dynamics, Inc., Madison, Wisconsin, USA).

To collect the three cell types, we used Trypsin–EDTA 0.25% Gibco, ThermoFisher Scientific, Waltham, MA, USA). To count cells, Trypan Blue Solution 0.4% (Gibco, ThermoFisher Scientific, Waltham, MA, USA) was added to cell suspensions. NucBlueTM Live Cell Stain ReadyProbesTM reagent (Hoechst 33 342, Invitrogen, ThermoFisher Scientific, Carlsbad, CA, USA) was added to the cells to identify the nuclei, while the Live/Dead® Viability/Cytotoxicity Kit (Invitrogen, ThermoFisher Scientific, Carlsbad, CA, USA) was used to label live and dead cells.

Cells were fixed in Formalin solution 10% neutral buffer (Sigma-Aldrich, Darmstadt, Germany), then washed using sodium azide (Sigma-Aldrich, Darmstadt, Germany) and permeabilised using Triton X-100 solution (Sigma-Aldrich, Darmstadt, Germany) and blocked with bovine serum albumin (Sigma-Aldrich, Darmstadt, Germany). Human coronary artery endothelial cells were stained with Purified Mouse Anti-Human CD31 (BD Pharmigen™, BD Biosciences, Cat# 550 389, Lot# 0079029) and Alexa Fluor® 647-conjugated AffiniPure Goat Anti-Mouse IgG (H + L) (Jackson

ImmunoResearch Laboratories, Inc., West Grove, Pennsylvania, USA), human CFs were stained with Alexa Fluor® 488 Mouse monoclonal Antibody to Vimentin [V9] (ab195877) (abcam, Cambridge, Cambridgeshire, UK). Human induced pluripotent stem cell-derived cardiomyocytes[2] were stained with Alexa Fluor® 546-conjugated Troponin T-C (CT3, sc-20025 AF546) (Santa Cruz Biotechnology, Dallas, Texas, USA).

2.1. SF isolation and formation of an aqueous solution

An aqueous solution of SF was prepared from the silkworm Bombyx mori cocoon thread (purchased from Sato Yama, Japan) through a three-step procedure as per our previously established protocols [29, 30]. Briefly, 5 g of delaminated silk samples were degummed using 0.02 M sodium carbonate (Na_2CO_3, Sigma Aldrich) in 2 l water at high temperature (90 °C–100 °C), to remove sericin from SF . First, degummed fibres were rinsed in water and dried under a fume hood. Then, they were dissolved in 9.3 M lithium bromide (LiBr, Sigma Aldrich) at 60 °C (4 ml/1 g fibres). Finally, a dialysis process using a cellulose membrane (1 cm/3 ml SF solution) (SnakeSkinTM Dialysis Tubing, Thermofisher scientific) and a 3-cycle centrifugation (8700 rpm, 4 °C, 15 min each step) was performed. The SF solution obtained was 7%–9% (w/v). SF solution was then stored at 4 °C before its use.

2.2. SF-containing hybrid hydrogel preparation, gelation and crosslinking

4% (w/v) Alg–8% (w/v) Gel hydrogels were prepared in a biosafety cabinet under sterile conditions according to our previously published protocol [5]. Briefly, sodium alginate (Alg, Sigma Aldrich) and gelatin (Gel, gelatin from bovine skin, Sigma Aldrich) powders were mixed under gentle rotation at 60 °C into 100 ml of Dulbecco Modified Eagle's Medium-high glucose (DMEM, Sigma Aldrich), containing 1% (v/v) penicillin-streptomycin (Sigma Aldrich) and 1% (v/v) L-glutamine (Sigma Aldrich). Hybrid hydrogels containing SF were prepared by mixing stock SF water solutions with Alg–Gel hydrogels that contained either a 1% (w/v) or a 2% (w/v) SF final concentration. 0% (w/v) SF hydrogels were prepared as well as control 4% (w/v) Alg-8% (w/v) Gel hydrogels. Hybrid hydrogels were stored at 4 °C until use.

A 2% (w/v) calcium chloride ($CaCl_2$, Sigma Aldrich) solution in Dulbecco's Phosphate Buffered Saline (DPBS, Sigma Aldrich) was prepared to crosslink Alg-containing hydrogels.

2.3. SEM and sample preparation

First, crosslinked hydrogels were prepared in a 96 well plate. Then, SF-containing hydrogels were incubated at 37 °C with DMEM cell culture medium up to 28 d. Before imaging, samples were dried overnight using a vacuum oven (Gallenkamp Vacuum Oven OVA031.XX1.5). Finally, hydrogels were coated with gold/palladium (Au/Pd) using a sputtering and carbon thread coater machine (Leica EM ACE600 Sputter Coater) and imaged using the Zeiss EVO scanning electron microscope. SEM images of SF-containing hydrogels were acquired through Zeiss SmartSEM software and at least 10 random areas from each SF-containing hydrogel region ($n \geqslant 6$), for each day of incubation were used for measurements [3]. The areas for each SF-containing hydrogel region were analyzed through ImageJ software (NIH Fiji), in order to measure the pore size of the hydrogels (supplementary figure 2).

2.4. Mechanical characterization of SF-containing hybrid hydrogels

As previously done in 4%Alg–8%Gel hydrogels, the mechanical properties of SF-based hybrid hydrogels were assessed using two complementary technologies: Brillouin spectroscopy and compression/rheology testing using a standard rheometer [24–26].

2.4.1. Brillouin spectroscopy

The Brillouin microspectroscopy system was identical to that reported by us previously [3]. The samples for Brillouin spectroscopy analysis were added to two 48-well plates to test two different conditions: samples before and after the 48 h crosslinking process. Each hydrogel condition had 3 repeats ($n = 3$). Brillouin measurements were taken at random points within three samples for each SF concentration and the measurement data were fitted using a Damped Harmonic Oscillator model. The Brillouin frequency shift (BFS) value was taken as the average between the Stokes and anti-Stokes frequencies in order to remove possible laser frequency drift [31]. Each measurement was repeated 3 times and the data were analyzed using Ghost 7.00 software. The data reported here represents the average across all repeats for each SF concentration.

2.4.2. Compression and rheology testing

Liquid samples were prewarmed at 37 °C and 500 μl were pipetted on the bottom plate geometry of the rheometer. Three samples for each SF hydrogel concentration ($n = 3$) were compressed between the two parallel plate geometries with a diameter of 25 mm, until the top one was touching the hydrogel surface. Tests were performed applying shear stress using a TA Instruments Dynamic Hybrid Rheometer (DHR-3, TA Instruments) and data were acquired through TRIOS Data acquisition software. The plate geometries were set first at 30 °C and then a temperature sweep from 30 °C to 4 °C was applied, with a temperature change of 3 °C min^{-1}. The oscillation strain (%) applied was between 0.2% and 2% of 360° of rotation and the angular frequency was set on the rheometer at 1 rad s^{-1} for the test at 30 °C and at 10 rad s^{-1} for the test at 30 °C–4 °C.

Solid samples for compression and rheology testing were prepared in two different 6-well plates, in order to test two different conditions: samples before crosslinking, which are those after gelation, and samples after crosslinking. Following gelation and overnight crosslinking (following the procedure described above), four punch biopsies ($n = 4$) of 8 mm in diameter were prepared for each SF-based hydrogel. Tests were performed through unconfined compression and applying shear stress using a TA Instruments Dynamic Hybrid Rheometer (DHR-3, TA Instruments) and data were acquired through TRIOS Data acquisition software. The mechanical characterization was performed by placing the 8 mm diameter punch biopsies between the two parallel plate geometries of the instrument. The samples were compressed up to 0.1 N axial force, thus not damaged, and the rate of deformation applied was constant at 10 μm s^{-1}.

The software collected data relative to the axial force applied on the sample's surface (cross-section area, m^2) and the rate of deformation (μm). To analyze compression data, the stress (Pa) and strain data were calculated and the analysis derived from these values resulted in a linear regression of the stress-strain curve, which was reproduced in Excel. The calculated slope of the linear region was characteristic of the compressive modulus (or Young's modulus) [24].

The stress and strain values were calculated using the following equations:

Strain = ratio of deformation = x_0–x_i/x_0
x_0 = deformation at the beginning of compression (μm)
x_i = step of sample deformation (μm)

Stress (Pa) = load = | Fi |/Cross section area
Fi = axial force (N) applied on sample surface
Cross section area (m^2) = $r^2 * \pi$

When measuring shear strain, the storage modulus (or shear elastic, G', MPa) and loss modulus (or shear viscous, G'', MPa) values resulted directly from the instrument and they derived from the oscillatory shear stress applied to the hydrogel. The samples were compressed between the plate geometries of the rheometer, up to 0.1 N axial force with a rate of deformation of 10 μm s^{-1} (as described above). During the rheometric measurements, the plate geometries were rotating on the samples (360° rotation) resulting in an oscillation strain (%) between 0.2% and 2% of 360° of rotation. The angular frequency (rad s^{-1}), which corresponds to the speed of oscillation, was set on the rheometer at 1 rad s^{-1} [24]. The whole experiment was performed at room temperature (25 °C) and the values of compression, shear elastic and viscous moduli compare the average across four measurements for each SF hydrogel.

2.5. Printability and durability of 3D bioprinted SF-containing hybrid hydrogels

SF-containing hybrid inks were 3D bioprinted using a BIO X6 extrusion-based bioprinter (CELLINK, Sweden). Pre-warmed three ml of hydrogels were loaded into a cartridge and at least six replicates for each SF concentration ($n \geqslant 6$) were extruded through a 22-gauge size nozzle into 6 well plates. Samples were bioprinted as a lattice of 20 mm × 20 mm × 0.82 mm (width × length × height) with two layers of 0.41 mm, which was designed using the DNA Studio 4 software (CELLINK, Sweden) with a rectilinear pattern and infill density of 25%.

The hydrogels printability was calculated using ImageJ software (NIH Fiji); multiple ($n \geqslant 6$) images of the width of the extruded hydrogel filaments were analyzed and a ratio between the measured values of the widths and the internal diameter of the nozzle was measured. Following gelation and one-hour crosslinking processes (described above), DMEM cell culture medium was added to each well and 3D bioprinted hydrogels were incubated at 37 °C in 5% (v/v) CO_2 in air for over 28 d. Cell culture medium was replaced with fresh medium every 4 d and hydrogels were imaged at different time points: after 1 d, 7 d, 14 d and 28 d from the day they were 3D bioprinted (day 0) [5].

2.6. Contractile activity and cell viability of CSs embedded in SF-containing hybrid hydrogels

CSs were prepared and analyzed as previously described [32]. Briefly, human coronary artery endothelial cells (HCAECs, Cell Applications, Inc., San Diego, CA, USA) and human CFs (HCFs, Cell Applications, Inc., San Diego, CA, USA) were cultured in T-flasks using MesoEndo Cell Growth Medium (Sigma Aldrich) for HCAECs and CF Growth Medium (Sigma Aldrich) for HCFs and incubated at 37 °C in 5% (v/v) CO_2 in air. Cell culture media were changed every 2 or 3 d and cells were detached using trypsin-EDTA (Sigma Aldrich) when cells reached 70%–80% confluency. Human induced pluripotent stem cell-derived cardiomyocytes^2 (hiPSCs-CMs, iCells^2, Fujifilm Cellular Dynamics, Inc., Madison, Wisconsin, USA) were cultured on fibronectin pre-coated flasks using iCell Cardiomyocytes Plating Medium (Fujifilm Cellular Dynamics, Inc., Madison, Wisconsin, USA). After 2 d, Plating Medium was replaced with iCell Cardiomyocytes Maintenance Medium (Fujifilm Cellular Dynamics, Inc., Madison, Wisconsin, USA).

CSs were generated by mixing hiPSCs-CMs, HCAECs and HCFs in a 2:1:1 ratio. 30 000 cells per spheroid were plated in 81 wells non-adherent 2% (w/v) agarose (Sigma Aldrich) micro-moulds, casted in 3D Petri Dish® (Sigma Aldrich). The micro-moulds were placed in 12 well plates and submerged using CSs medium, which was prepared by mixing iCell Cardiomyocytes Maintenance Medium, MesoEndo

Cell and CF Growth Media in a 2:1:1 ratio. CSs medium was replaced every 2 d.

CSs were plated in 96 well plates; at least three spheroids ($n \geqslant 3$) were plated in each well and SF-containing hybrid hydrogels were added on top of the spheroids. Following gelation and one-hour cross-linking processes (described above), CSs medium was added to the wells and well plates were incubated at 37 °C in 5% (v/v) CO_2 in air. CSs medium was replaced every 2 d with fresh medium up to 28 d. At the 28th day, CSs were recorded using EVOS M7000 Cell Imaging System (ThermoFisher Scientific) microscope. These videos were used to measure the contraction frequency (number of contractions of the CSs per second) and the fractional shortening % (FS%). The latter was calculated using the following formula:

$$(\mathrm{Dc} - \mathrm{Dr})/\mathrm{Dc}$$

where 'Dc' corresponds to the diameter of the contracted spheroid and 'Dr' to the one of the relaxed spheroids. Then CSs were stained with Hoechst dye (Nuc Blue Life Technologies), calcein-AM and ethidium homodimer (Live/Dead®, Invitrogen, Carlsbad, CA, USA), to identify cell nuclei and detect live and dead cells respectively [5]. Following 3 h of incubation at 37 °C with calcein-AM and ethidium homodimer, CSs were imaged through LAS X imaging software using an LSCM Leica Stellaris DMI-8 confocal microscope (Leica Mycrosystems) and images were analyzed using ImageJ software (NIH Fiji) in combination with Adobe Photoshop CC (Adobe Systems, Inc., San Jose, CA, USA).

2.7. Immunostaining of CSs embedded in SF-containing hybrid hydrogels

CSs in hydrogels were stained as previously described [3, 5]. Briefly, at least three replicates ($n \geqslant 3$) of CSs embedded in SF-containing hybrid hydrogels were fixed with 10% neutral buffered formalin solution (containing 4% formaldehyde) (Sigma Aldrich) and incubated at 4 °C overnight. Following 3x washes using 0.01% (v/v) PBSA (PBS containing 0.01% (v/v) sodium azide), samples were permeabilized using 0.02% (v/v) Triton X-100 solution and blocked by adding 3% (w/v) bovine serum albumin (BSA) in 0.01% (v/v) PBSA to the wells. Samples were incubated at 4 °C overnight [5]. Then, CSs were immunostained using primary purified mouse anti-human CD31 antibody (5 μg ml^{-1}, BD PharmigenTM, BD Biosciences) to label HCAECs, and samples were incubated at 4 °C overnight. The following day, samples were first washed using 0.01% (v/v) PBSA and incubated with the secondary antibody Alexa Fluor® 647-conjugated goat anti-mouse (10.5 μg ml^{-1}, Jackson ImmunoResearch Laboratories, Inc., West Grove, Pennsylvania, USA) in the dark at 4 °C overnight. CSs were also immunostained with monoclonal antibody Alexa Fluor® 488 (1 μg ml^{-1}, abcam) against Vimentin, for HCFs, and using Troponin T-C, Alexa Fluor® 546-conjugated (16.7 μg ml^{-1}, Santa Cruz Biotechnology) for cardiac troponin, thus CMs, together with Hoechst dye (4 drops ml^{-1}, Nuc Blue Life Technologies). Samples were incubated in the dark at 4 °C overnight. Between each step, samples were washed using 0.01% (v/v) PBSA and after adding the antibodies, well plates were placed on ice on a rocking plate at 60 rpm. Samples were then imaged through LAS X imaging software using an LSCM Leica Stellaris DMI-8 confocal microscope (Leica Microsystems), by capturing Z-stack images [32]. The fluorescence was analyzed through ImageJ software (NIH Fiji) in combination with Adobe Photoshop 2023 (Adobe Systems, Inc., San Jose, CA, USA).

2.8. Statistical analyses

Results were plotted in GraphPad Prism™ (La Jolla, CA) and statistical significance of the analyses was assessed using a Brown–Forsythe and Welch ANOVA test, together with a Dunnett's T3 multiple comparisons test. Each error bar is representative of the standard error mean of the average value; for SEM and contractile activity values, the median value is showed. Durability results were calculated using a Kaplan-Meier Survival curve Log-rank (Mantel-Cox) test, together with a Gehan–Breslow–Wilcoxon test.

3. Results

3.1. Hydrogel pore size decreases with increased SF concentrations to Alg–Gel hydrogels

In order to evaluate the potential role played by SF in controlling the mechanical properties of previously established Alg–Gel hydrogels for cardiovascular applications [3], we first generated hybrid hydrogels containing 1% and 2% SF. We decided to test these specific SF concentrations based on previous studies [5, 8, 18, 29, 33, 34].

These hydrogels were then characterized via SEM to evaluate if the addition of SF may control their pore size, which are important to maintain proper oxygen and nutrient exchange [3]. Our analyses showed that increasing SF concentrations reduce the size of the pores in Alg–Gel hydrogels starting from one day in cell culture medium (figure 2). The addition of 1% SF to 4%Alg–8%Gel hydrogels decreases the pore size by 40%, 49%, 10% and 38% at 1, 7, 14 and 28 d, respectively (figures 2(A)–(D)). The addition of 2% SF reduced the pore size of Alg–Gel hydrogels by 65%, 83%, 79% and 69% at 1, 7, 14 and 28 d, respectively (figures 2(A)–(D)).

3.2. The addition of SF to Alg–Gel formulations modulates their mechanical properties

In order to evaluate if SF can alter the mechanical properties of Alg–Gel hydrogels, they were analyzed using both Brillouin microspectroscopy and classic

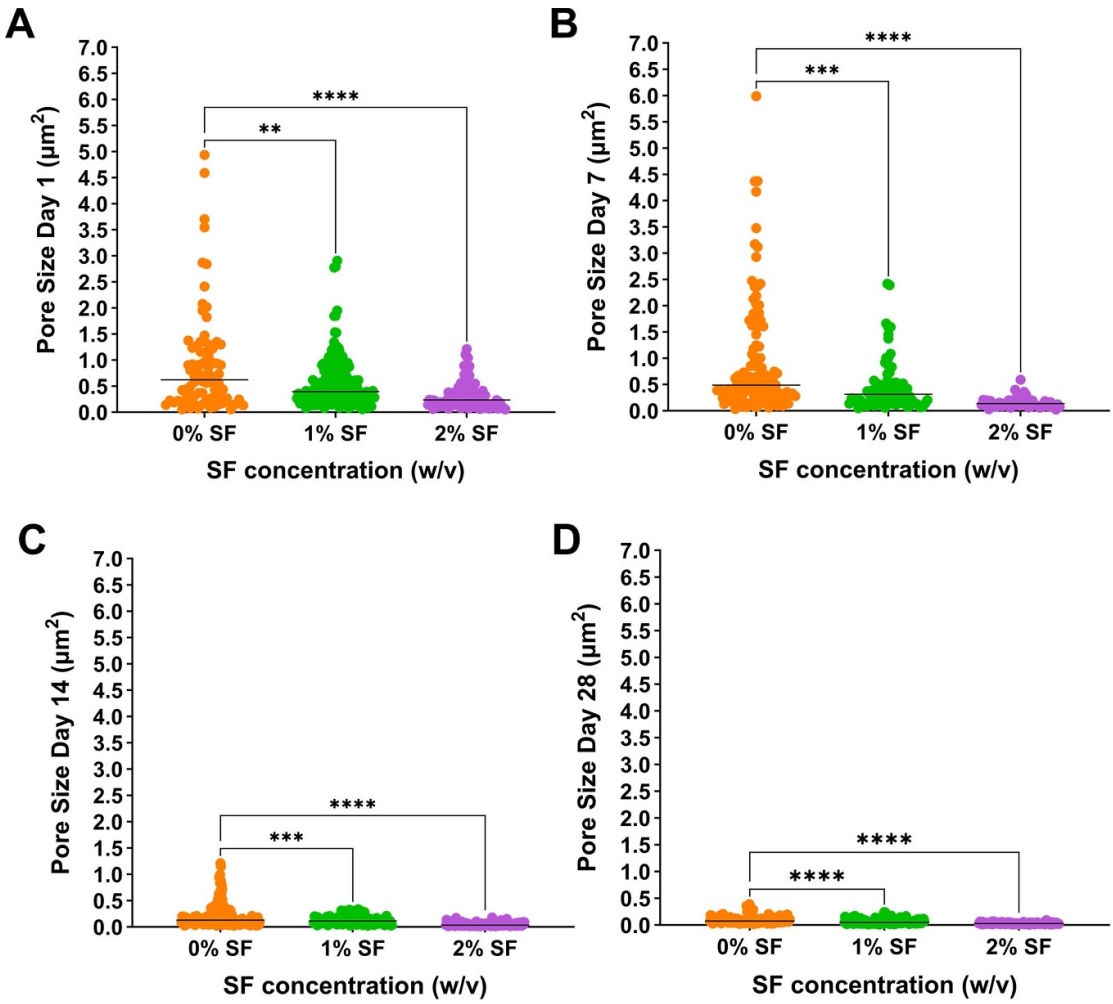

Figure 2. Microstructural changes following SF addition to Alg–Gel hydrogels. (A)–(D) Analyses of the pore size measurements for crosslinked 4%Alg–8%Gel hydrogels containing 0%, 1%, and 2% SF concentration, after 1 d (A), 7 d (B), 14 d (C) and 28 d (D) of incubation with cell culture medium at 37 °C in 5% (v/v) CO_2 in air. The statistical analyses performed on Alg–Gel–SF hydrogels includes a Brown–Forsythe and Welch ANOVA test, together with a Dunnett's T3 multiple comparisons test. Data are represented as the median (** $p < 0.01$, *** $p < 0.001$ **** $p < 0.0001$, $n \geqslant 6$).

rheology as complementary [3]. Brillouin microspectroscopy directly measures the speed of hypersound waves within the sample that in turn can be related to the sample's local elasticity and viscosity [22, 26, 35]. Brillouin measurements of samples with increasing SF concentration (0% (w/v), 1% (w/v) and 2% (w/v) SF) were performed before (figure 3(A)) and after (figure 3(B)) crosslinking. The statistical analysis shows that the BFS detected for non-crosslinked samples (figure 3(A)) increases with the addition of SF, equating to 0.05 ± 0.002 GHz difference between hydrogels containing 0% SF and 1% SF, whereas 2% SF hydrogels show an increment of BFS equal to 0.05 ± 0.005 GHz difference. This increment in the BFS is relatively small compared to the result obtained for crosslinked hydrogels (figure 3(B)), where the BFS between 0% SF and 2% SF hydrogels increases by 0.12 GHz. This indicates that the addition of SF into hydrogel suspension does not lead to significant changes in mechanical properties as the result of the gelation process only (i.e. a crosslinking stage was required to form molecular bonds within hydrogel material and to induce an elastic response).

As SF-containing hydrogels are designed to be employed for 3D bioprinting of cardiac tissues, standard rheology was performed on liquid (supplementary figure 3) hydrogels. This helped to analyse the elasticity and viscosity of the materials at the temperature of bioprinting while in a liquid form (30 °C). In addition, we also analyzed the rheological properties of the hydrogels during gelation at lower temperatures (down to 4 °C, supplementary figure 3) and after crosslinking (figure 4).

Before gelation (at 30 °C), the shear elastic (G', supplementary figure 3(a)) and shear viscous (G'', supplementary figure 3(B)) moduli are quite low (<0.001 kPa for all measurements) compared to their solid form and the results are not statistically different after the addition of SF; however, the shear viscous modulus (supplementary figure 3(B)) is always higher than the shear elastic modulus (supplementary figure 3(A)), which is an expected

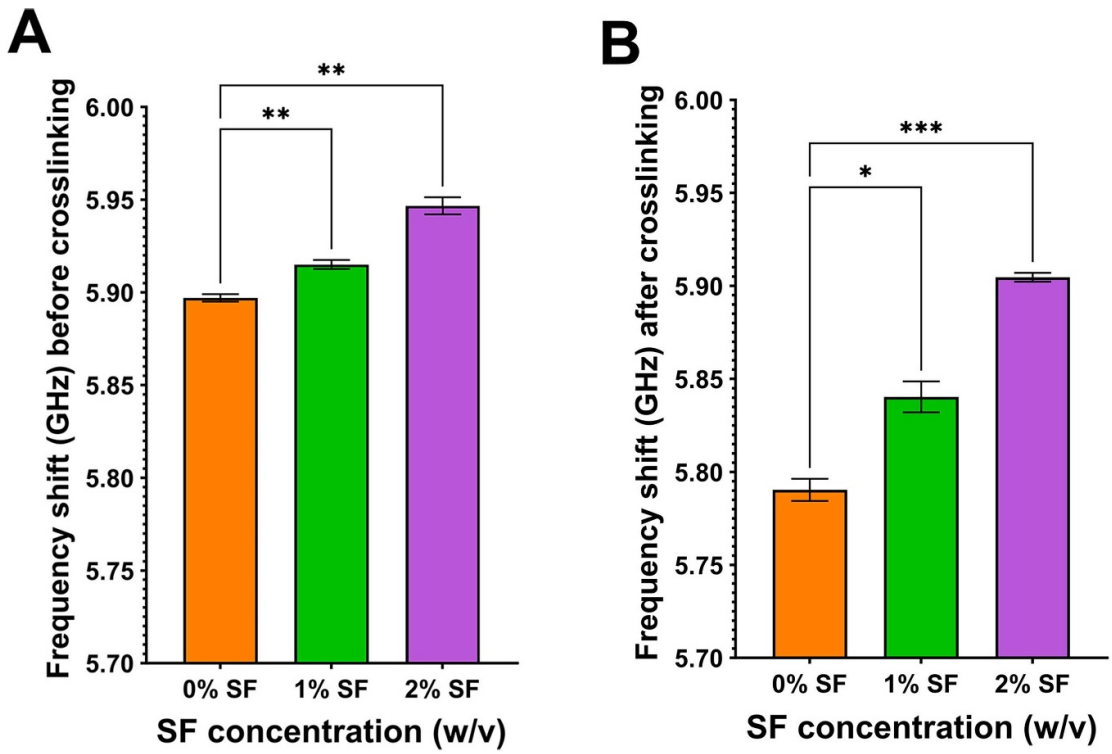

Figure 3. Brillouin spectroscopy of Alg–Gel–SF hydrogels.(A)–(B) Analyses of Brillouin microspectroscopy frequency shift (GHz) measurements of Alg–Gel–SF hydrogels before (A) and after (B) crosslinking. The values for each SF concentration represent the average across three measurements of three hydrogels. The statistical analyses performed on Alg–Gel–SF hydrogels includes a Brown–Forsythe and Welch ANOVA test, together with a Dunnett's T3 multiple comparisons test. Data are represented as mean with standard error mean (* $p < 0.05$, ** $p < 0.01$, *** $p < 0.001$, $n = 3$).

behavior for hydrogels when they are in a liquid form.

During gelation (between 30 °C and 4 °C) (supplementary figures 3(C)–(F)) show that at 30 °C the shear viscous modulus is higher than the shear elastic one; once the temperature starts decreasing gradually until 4 °C, the trend of both moduli changes and the shear elastic modulus becomes higher than the viscous one. The crossover points between the shear elastic and viscous moduli, which correspond with the point when hydrogels start to solidify, are 19 °C for all SF-containing hydrogels. supplementary figures 3(C)–(E) show the trend of both shear elastic and viscous moduli of 0% SF (supplementary figure 3(C)), 1% SF (supplementary figure 3(D)) and 2% SF (supplementary figure 3(E)) hydrogels during a temperature sweep between 30 °C and 4 °C. supplementary figure 3(f) represents all values of shear elastic and viscous moduli that are already shown in supplementary figures 3(C)–(E).

Rheology and compression tests were performed on both non-crosslinked (figures 4(A) and (C), respectively) and crosslinked hydrogels (figures 4(B) and (D), respectively).

When evaluating changes in rheological properties due to crosslinking (figure 4), the shear elastic modulus of SF-containing hydrogels before crosslinking does not significantly change with the addition of SF (figure 4(A)). However, the shear elastic modulus significantly increases after crosslinking with increasing concentrations of SF (figure 4(B)). The shear viscous modulus increases only after the addition of 2% SF compared to 0% before crosslinking (figure 4(C)) and after crosslinking (figure 4(D)).

Similar to the outcomes of shear elastic modulus measurements and Brillouin spectroscopy measurements, Young's modulus increases proportionally with the addition of SF concentration before (figure 4(E)) and after (figure 4(F)) crosslinking. Only the addition of 2% SF significantly increased the Young's moduli before crosslinking (figure 4(E)). After crosslinking, Young's modulus increased proportionally with the addition of SF, but it was not statistically significant (figure 4(F)). Altogether, our findings show that the addition of SF alters the mechanical properties of Alg–Gel hydrogels only after crosslinking.

3.3. Increasing SF concentrations improve the printability and durability of Alg–Gel hydrogels

To assess the printability and durability of SF-containing hybrid hydrogels [5], we 3D bioprinted SF-containing hybrid hydrogels using an extrusion-based BIO X6 (CELLINK Life Sciences) bioprinter (supplementary videos 1(A)–(C)). Hybrid hydrogels containing 4% (w/v) Alg, 8% (w/v) Gel at different SF concentrations (0% (w/v), 1% (w/v) and 2% (w/v) SF) were 3D bioprinted on day 0 in 6 well plates with

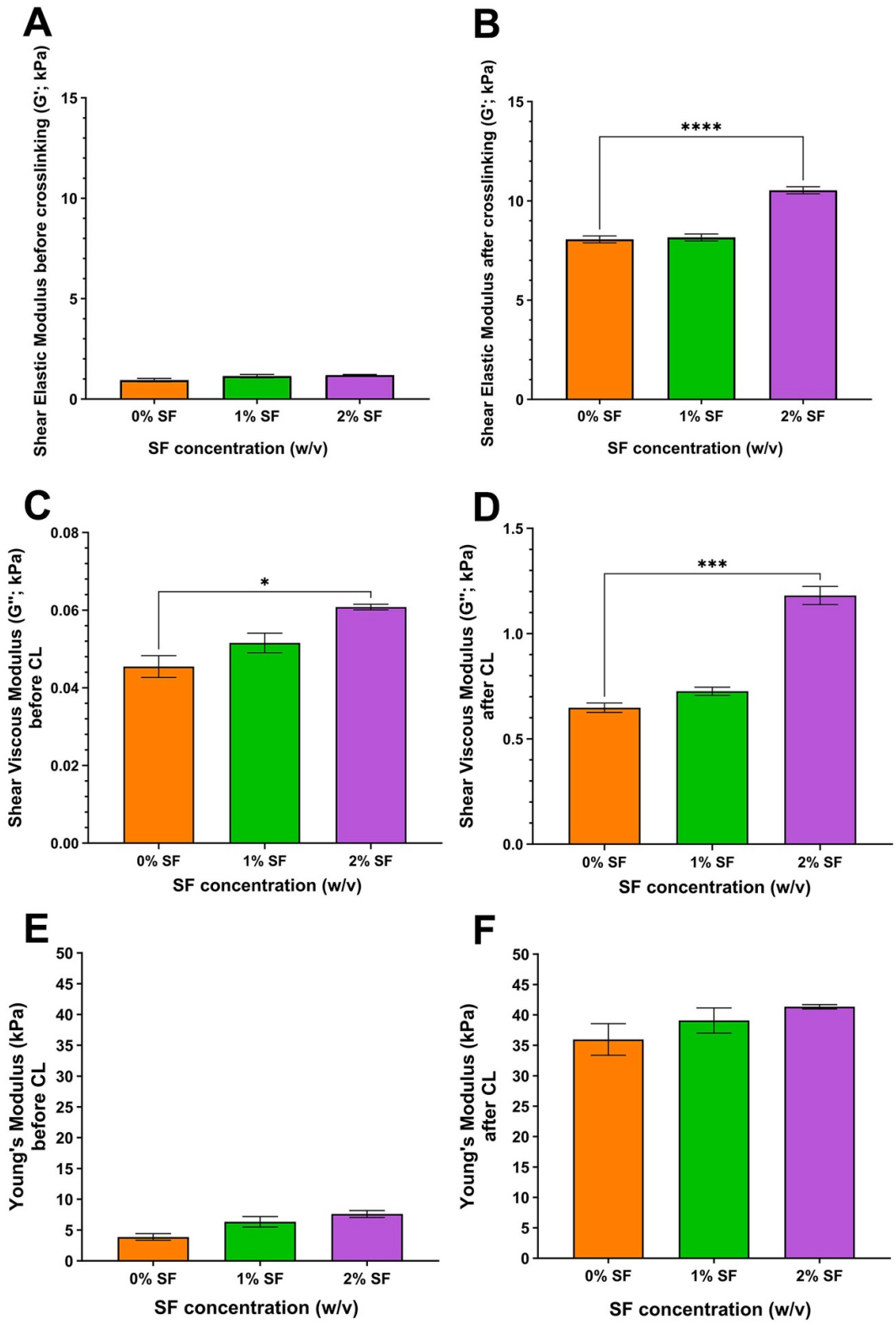

Figure 4. Rheometric measurements of solid Alg–Gel–SF hydrogels.(A)–(D) analyses of rheometric measurements characteristic of the shear elastic moduli before (A) and after (B) crosslinking, and the shear viscous moduli before (C) and after (D) crosslinking of SF-based hybrid hydrogels. (E)–(F) analyses of compression testing measurements characteristic of Young's moduli before crosslinking (E) and after crosslinking (F) of SF-based hybrid hydrogels. The values are characteristic of the average between measurements performed on four not-crosslinked (A), (C) and (E) and four crosslinked (B), (D) and (F) samples for each SF concentration. The statistical analyses performed for mechanical characterization of Alg–Gel–SF hydrogels include Brown–Forsythe and Welch ANOVA tests, together with Dunnett's T3 multiple comparisons tests. Data are represented as means with standard error means (** $p < 0.01$, **** $p < 0.0001$, $n = 4$, CL = crosslinking).

at least 6 replicates per group. These were bioprinted in a four-squares construct through a rectilinear pattern.

The analysis of printability of 3D bioprinted SF-containing hybrid hydrogels is shown in the plot (figure 5(A)), which is representative of normalised

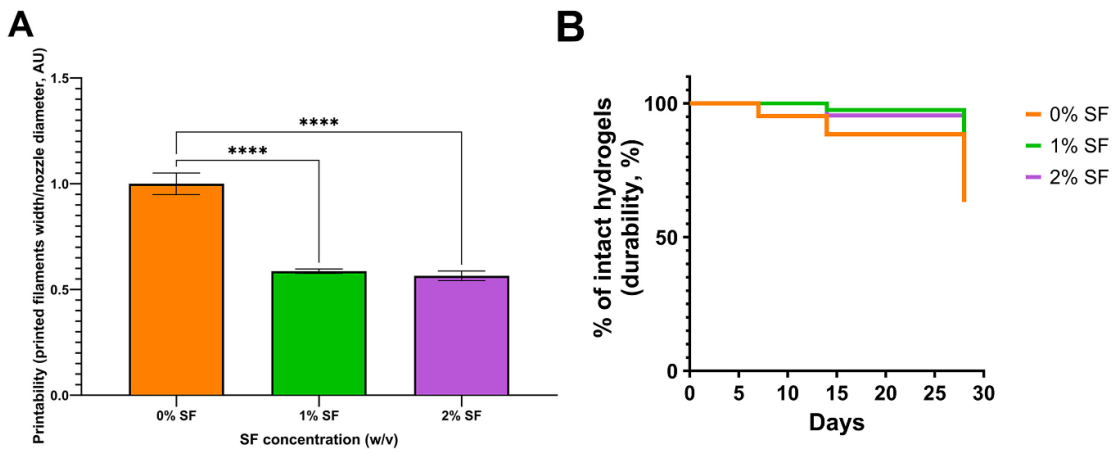

Figure 5. Printability and durability of Alg–Gel–SF hydrogels. (A)–(B) Analyses of the printability and durability of Alg–Gel–SF hybrid hydrogels. (A) The plot is characteristic of the printability of 4%Alg/8%Gel hydrogels with varying concentrations of SF. It represents normalised values of the ratios between the measures of the widths of the 3D printed filaments at day 0, before crosslinking, and the internal diameter of the nozzle. The statistical analysis performed includes a Brown–Forsythe and Welch ANOVA test, together with a Dunnett's T3 multiple comparisons test. Data are represented as mean with standard error mean (**** $p < 0.0001$, $n \geqslant 6$; 0% SF ($n = 7$), 1% SF ($n = 20$), 2% SF ($n = 11$)). (B) The plot shows the durability of the 3D printed structures in cell culture medium at day 7, 14 and 28, meant as a percentage of intact hydrogels. It indicates the specific days, where the 3D printed structures did not preserve their shape. The statistical analysis performed includes a Log-rank (Mantel–Cox) test, together with a Gehan–Breslow–Wilcoxon test ($n \geqslant 6$; 0% SF ($n = 7$), 1% SF ($n = 20$), 2% SF ($n = 11$)).

data of the ratio between the width of extruded filaments and the internal diameter of the nozzle. The values of the width of printed filaments are compared with the measure of the nozzle diameter (0.41 mm); considering the nozzle diameter as the ideal printability of the filaments (the closer the value is to 0.41 mm, the more printable it is). The statistical analysis of the printed hydrogels shows an increase in printability and fidelity shape proportional to the addition of SF to Alg–Gel hydrogels (supplementary figure 4).

The durability of the 3D bioprinted Alg–Gel–SF hydrogels in cell culture medium was evaluated visually over 28 d at different time points: after 1 d, 7 d, 14 d and 28 d from the day of bioprinting (day 0) (figure 5(B)). At least 90% of the bioprinted hybrid hydrogels containing SF were durable and they did not dissolve in cell culture medium. The addition of 1% and 2% SF to 4%Alg–8%Gel hydrogels improved their durability by 21% and 22% after 28 d, respectively.

3.4. The addition of SF to Alg–Gel hydrogels regulates the contractile activity and affects cell viability of CSs embedded in SF-containing hybrid hydrogels

To evaluate the possible role of SF in supporting and enhancing the viability and function of human cardiac cells, in *vitro* CSs in Alg–Gel–SF hydrogels were cultured up to 28 d [3, 5].

The contractile activity of CSs embedded in SF-containing hydrogels (supplementary videos 2(A)–(C)) was analyzed at 28 d of incubation in cell culture medium. This includes the analysis of their contraction frequency (figure 6(A)), which corresponds to the number of contractions of the spheroids per minute, as well as the FS%, figure 6(B), which is related to the difference between the diameter of the contracted and relaxed spheroid. The addition of 2% SF led to a decrease in contraction frequency (figure 6(A)). The addition of 1% SF led to a FS% increase by 41%, representative of a stronger FS, which we never observed before (figure 6(B)). Furthermore, figures 6(C) and (D) are representative of the diameters of the CSs when are relaxed and contracted, respectively. For instance, relaxed CSs present a diameter average of 122 ± 4 mm, 101 ± 6 mm and 108 ± 8 mm when embedded in 0% SF, 1% SF and 2% SF hydrogels, respectively. Contracted CSs, instead, present a diameter average of 125 ± 4 mm, 105 ± 6 mm and 111 ± 8 mm when embedded in 0% SF, 1% SF and 2% SF hydrogels, respectively. In both cases, the data show that CSs diameters decreased, thus CSs size is reduced, by increasing SF concentrations to Alg–Gel hydrogels.

In addition, cardiac cell viability analysis was performed on CSs embedded in SF-containing hydrogels after 28 d in cell culture medium and 37 °C. The Live/Dead staining through calcein-AM and ethidium homodimer was used to identify live and dead cells respectively (figures 7(A)–(C)). Our results show that most of the cardiac cells contained in CSs survived when embedded in 4%Alg–8%Gel hydrogel (0% SF, figure 7(A)), as well as in 1% SF-containing hydrogels (figure 7(B)). 2% SF-containing hydrogels (figure 7(C)), instead, represent a less-friendly microenvironment for cardiac cell survival. The analysis of the CS toxicity ratio (figure 7(D)) is representative of data on the ratio between dead and live cells.

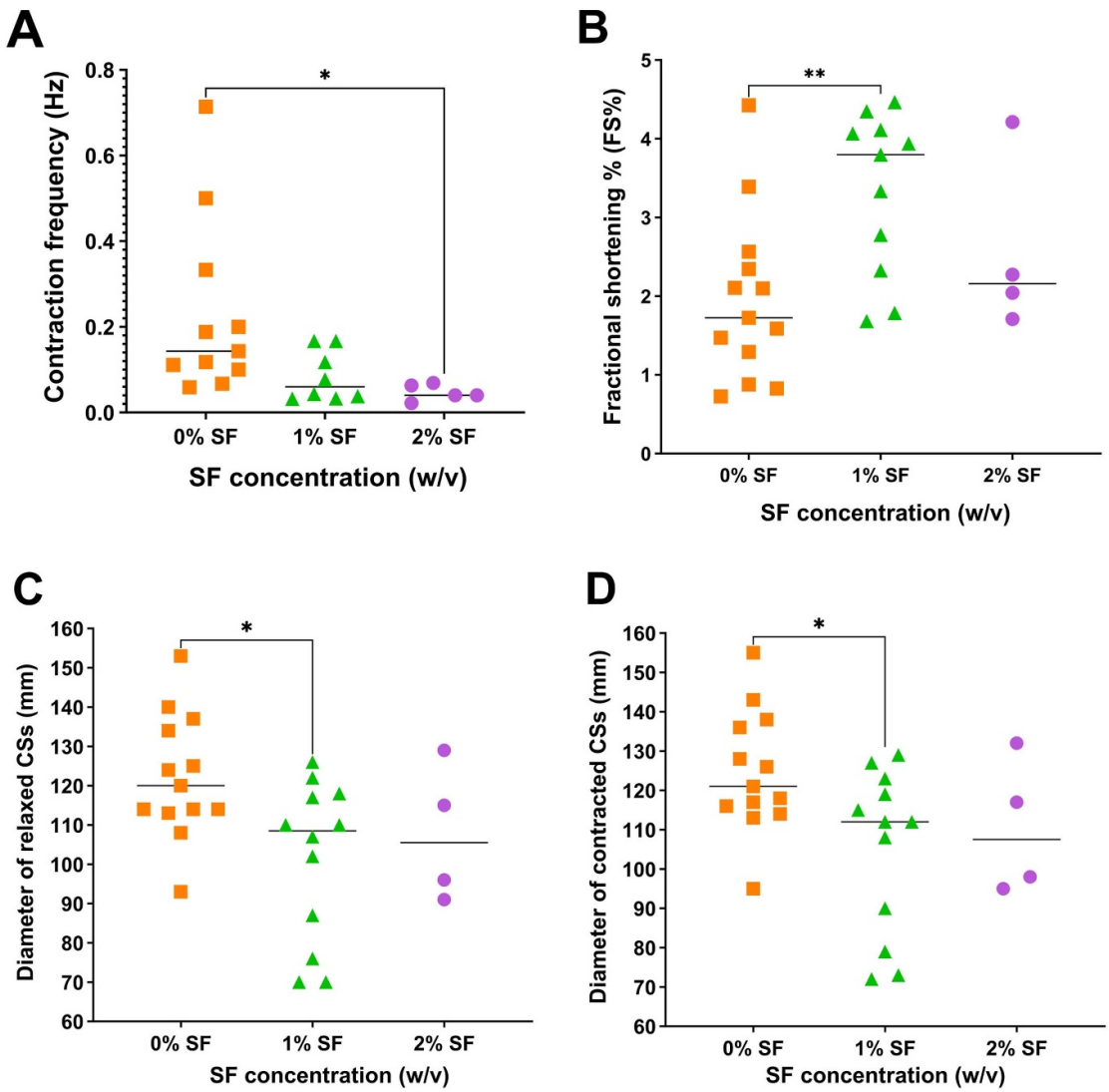

Figure 6. Contractile activity of encapsulated cardiac spheroids in Alg–Gel–SF hydrogels. (A)–(B) analyses of contraction frequency ((A), 0% SF ($n = 11$), 1% SF ($n = 8$), 2% SF ($n = 5$)) and their fractional shortening ((B), 0% SF ($n = 13$), 1% SF ($n = 11$), 2% SF ($n = 4$)) of cardiac spheroids encapsulated in 4%Alg–8%Gel hydrogels with different concentrations of SF (0–2%). The data derive from videos acquired through EVOS M7000 microscope after 28 d of incubation at 37 °C in cell culture medium. (C) analysis of the size of the spheroids when they are not contracted, thus the diameter of CSs when they are relaxed (0% SF ($n = 13$), 1% SF ($n = 11$), 2% SF ($n = 4$)). (D) Analysis of the size of the spheroids when they are contracted, thus the diameter of CSs when they are contracted (0% SF ($n = 13$), 1% SF ($n = 11$), 2% SF ($n = 4$)). The statistical analyses performed is a Brown–Forsythe and Welch ANOVA test, together with a Dunnett's T3 multiple comparisons test. Data are represented as the median (* $p < 0.05$, ** $p < 0.01$, $n \geqslant 3$).

Our statistical analysis showed that, while the addition of 1% SF did not significantly reduce the viability of cells, the addition of 2% was too high for cells to live in these hydrogels. As a comparison, we also report the percentage of dead cells versus total cells (supplementary figure 5), which is consistent with the toxicity ratio results. As a result of both our analyses of the contractile function and cell viability in SF hydrogels, we decided to select the 1%SF hydrogels for the next analyses.

3.5. The addition of SF to Alg–Gel formulations does not affect the cell distribution in CSs embedded in SF-containing hybrid hydrogels

We have previously demonstrated that Alg and Gel hydrogels are suitable to support cardiac endothelial cells (CECs) and CFs growth, as well as cardiomyocyte contractile activity within CSs (CMs) [3, 5]. To evaluate any effect of 1% SF on these cells, CSs embedded in Alg–Gel–SF hydrogels were stained using antibodies against CD31, cardiac troponin T and vimentin, which label CECs, CMs and CFs, respectively. Our analysis of CSs cultured for 28 d in their cell culture medium and either 0% or 1% SF hydrogels, stained with the cell-specific antibodies and imaged under a confocal microscope, confirmed the presence of CECs (CD31, red), CMs (cardiac troponin T, blue) and CFs (vimentin, green) (figures 8(A) and (B), respectively). Of note, the diameter of CSs in 1% SF is smaller than in 0%SF (figures 6(C), (D) and 8(B)), which was even smaller for CSs in 2%SF (figures 6(A) and (B)). Altogether, our analyses showed that 1%SF

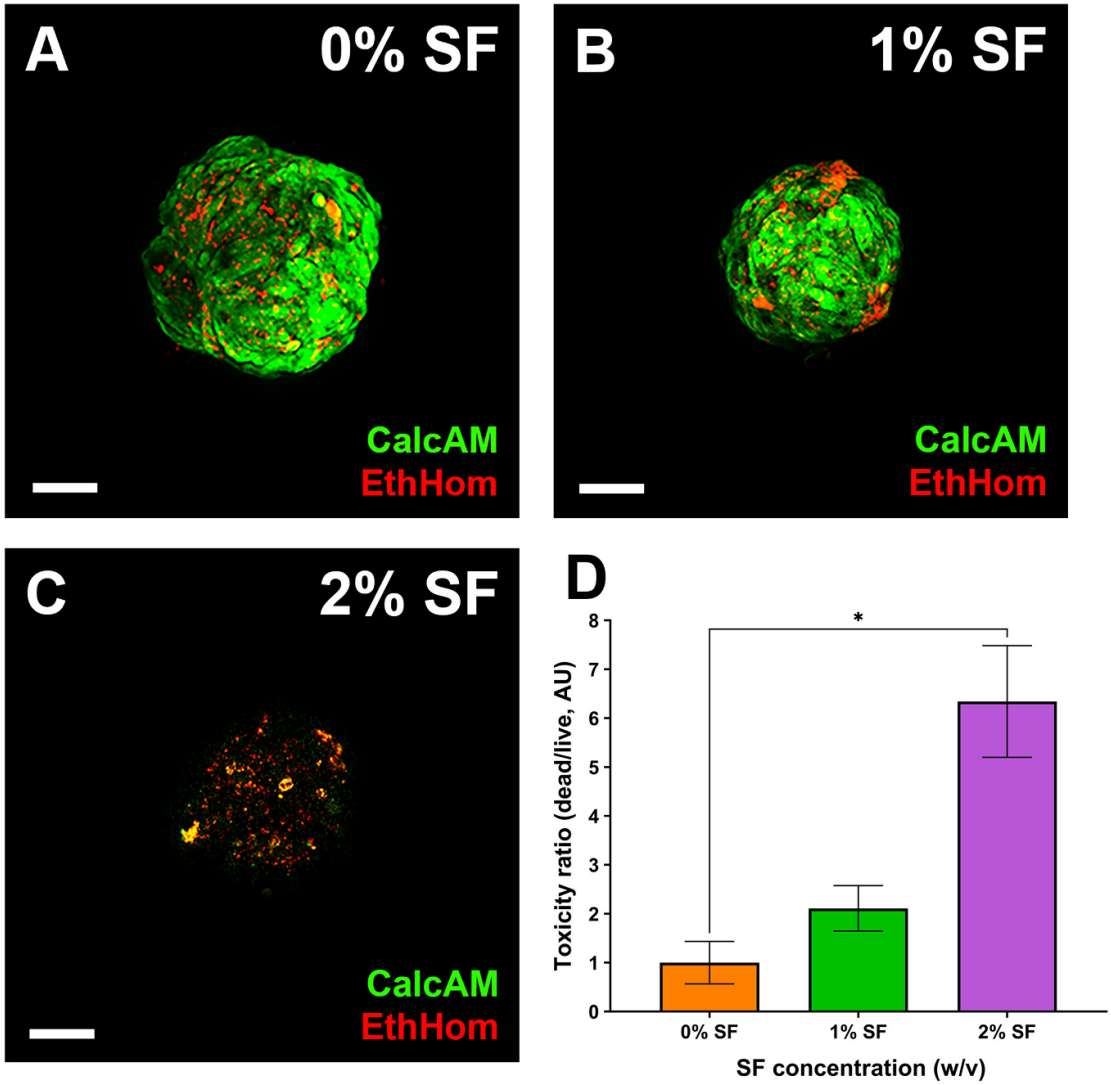

Figure 7. Toxicity ratio of encapsulated cardiac spheroids in Alg–Gel–SF hydrogels. (A)–(C) Representative images of cell viability of cardiac spheroids embedded in 4%Alg–8%Gel hydrogels with different concentrations of SF. The images are characteristic of collapsed Z-stacks of CSs and they represent the live (calcein-AM) and dead (ethidium homodimer) staining for CSs embedded in 4%Alg–8%Gel hydrogels containing 0% ((**A**), $n = 4$), 1% ((B), $n = 5$) and 2% ((C), $n = 3$) SF after 28 d of incubation at 37 °C in cell culture medium. (D) Statistical analyses of toxicity ratios (dead cells/live cells) of CSs embedded in the hybrid hydrogels. The statistical analysis performed is a Brown–Forsythe and Welch ANOVA test, together with a Dunnett's T3 multiple comparisons test. Data are represented as mean with standard error mean (* $p < 0.05$, magnification bar = 100 μm, $n \geqslant 3$).

can be added to Alg–Gel hydrogels to improve their contractile activity without affecting their viability.

4. Discussion

In this study, we reported for the first time the use of SF as bioink formulation for cardiac tissue engineering applications, despite previous attempts [1]. We aimed to test different concentrations of SF (0% (w/v), 1% (w/v), 2% (w/v)) mixed with 4%Alg–8%Gel hydrogels, which already showed optimal conditions for cardiac cells viability and contractile activity, *in vitro* and *in vivo* [3–5]. However, Alg–Gel hydrogels are characterised by limitations, such as limited durability in physiological conditions [5]. Given the SF tuneable mechanical features and low immunogenic response when transplanted in the human body [1, 36], we studied the role of SF in modulating the mechanical properties of Alg–Gel hydrogels, as well as in improving their printability. Our analyses demonstrated that the addition of SF reduced the pore size in Alg–Gel hydrogels, but it increased their elasticity (Figures 3(B) and 4(D)). By creating a hybrid Alg–Gel–SF bioink, we also solved the printability problem related to the low viscosity of pure SF aqueous solution, which was impossible to print.

Moreover, the addition of SF to Alg–Gel hydrogels allowed us to control the slow gelation and degradation rates of SF solutions, as well as the transition from α-helices to β-sheets due to the heat and shear thinning forces during the bioprinting process, which causes the occlusion of the nozzle [1, 37, 38]. Recent works also demonstrated that SF was extrudable at

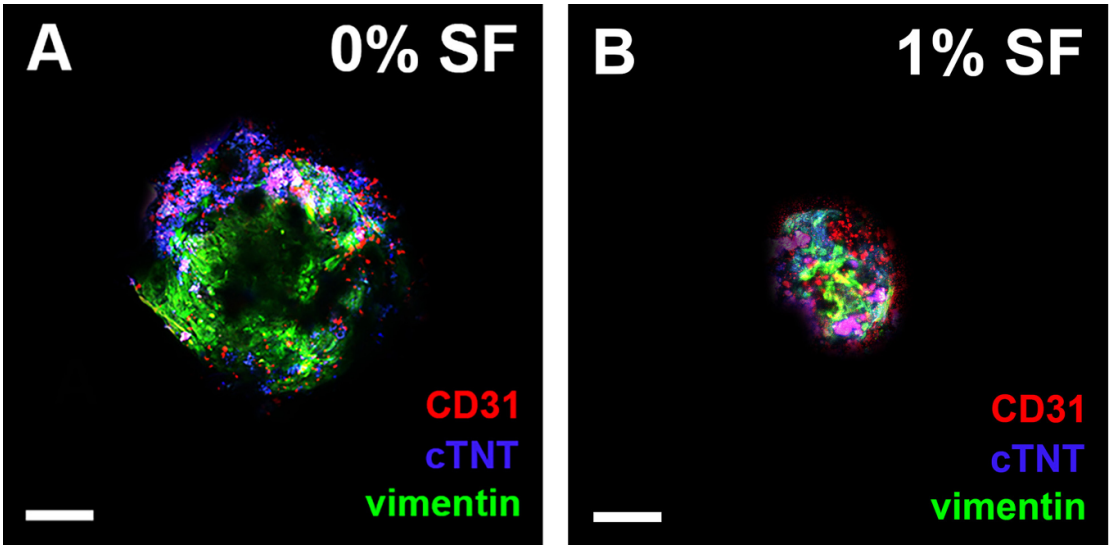

Figure 8. Cardiac endothelial cells, cardiomyocytes and cardiac fibroblasts presence in cardiac spheroids embedded in Alg–Gel–SF hydrogels. (A)–(B) Representative collapsed Z-stack confocal images of cardiac spheroids embedded in 4%Alg–8%Gel hydrogels containing 0% (A) and 1% (B) SF. Each CS was stained with antibodies against CD31 (cardiac endothelial cells, red), cardiac troponin T (cardiomyocytes, blue) and vimentin (cardiac fibroblasts, green) (magnification bar = 100 μm, $n \geqslant 3$).

low concentrations (2%–5% w/v) when combined with higher concentrations of natural-based biomaterials and this was necessary to achieve the required rheological features to bioprint SF solution [35, 39, 40]. In this regard, all of our SF-hydrid hydrogels were extrudable using an extrusion-based bioprinting system (supplementary videos 1(A)–(C)). This might be due to the ability of SF to bind with Alg allowing quick gelation [1, 20]. Furthermore, the addition of increasing concentrations of SF to 4%Alg–8%Gel hydrogels resulted in an improved printability and geometry fidelity of the 3D bioprinted constructs, compared to only 4%Alg–8%Gel hydrogels (figure 5(A) and supplementary figure 4). The addition of $CaCl_2$ to allow the crosslinking process of alginate within the Alg–Gel–SF hybrid hydrogels played a key role in fabricating a 3D structure with higher durability; this was likely caused by electrostatic interactions between calcium positive ions (Ca^{2+} ions) and SF negative charged amino acids present in the SF chains [41].

The addition of SF also changed the microstructure of Alg–Gel 3D constructs. Increasing SF concentrations decreased the pore size of the hydrogels between 7 and 28 d of incubation in cell culture medium (figures 2(B)–(D)). This is due to the formation of more polymer bindings between SF and Alg–Gel polymers, which is proportional to the amount of SF added, indicating a higher level of crosslinking and more compact hydrogel network, which may contribute to the reduction in pore size (figure 2) [42]. This might be responsible for less exchange of oxygen and nutrients, which is crucial for cell growth and proliferation within the hydrogel. The increased crosslinking may also be responsible for a reduction in space for cells to migrate in [43], which can also be linked to the reduced viability of cardiac cells at higher concentrations of SF (figure 7(C)).

Furthermore, higher SF concentrations in Alg–Gel hydrogels can also affect the water uptake capacity of the hydrogels, due to the hydrophobic properties of the β-sheets present in silk . The reduced pore size limits the accessibility of water molecules [44], indicating that hydrogels containing higher SF concentrations are less able to absorb and retain water and, thus less hydrated, which may have an impact on cell viability, reducing oxygen diffusion through the 3D structure [43].

Other important features to be considered for bioinks formulations are their mechanical properties. If rheology provides information on the Young's, shear elastic and shear viscous moduli averaged across the entire sample volume, Brillouin microscopy has the advantage of microscale resolution, although the outputs from Brillouin microscopy measurements differ from that of rheology and characterize material compressibility in the high-frequency regime of mechanical perturbation [45, 46]. The shear elastic modulus (figures 4(A) and (B)) and shear viscous modulus (figures 4(C) and (D)) represent the material's stiffness and viscoelastic properties and refer to the resistance of the material during a shear deformation, while Young's modulus is an unconfined compression modulus (figures 4(E) and (F)). It is important to note that the average value for Young's moduli was 5–7 times higher for crosslinked hydrogels (figure 4(F)) compared to those prior crosslinking (figure 4(E)), supporting the efficiency of the process in forming polymer network and stiffening the hydrogels.

The results of these two techniques (rheology and Brillouin spectroscopy) are often found to correlate but cannot be directly related to one another due to the complex structure of the multi-component hydrogel network. The BFS is directly proportional to the longitudinal modulus, which is related to the elastic properties of the hydrogels and has a meaning of inverse compressibility [31]. Following the addition of SF at increasing concentrations, an increase in frequency shift was measured, suggesting higher longitudinal modulus and lower compressibility of SF-rich hydrogels. This is consistent with our rheology and confined compression tests, which both show a positive correlation between SF concentration and the respective moduli. The effects are more pronounced in crosslinked hydrogels as expected, suggesting higher stiffness of the hydrogels [41]. This results in reduced compressibility of the hydrogels, with a direct influence on the frequency of contractile activity of CSs, leading to frequency reduction (figure 6(A)). Furthermore, the increase of hydrogel stiffness, which is consistent with a decrease in pore size (figure 2), also affects the number of cell adhesion sites [43]. Altogether, the increase of SF-containing hydrogel stiffness makes their pores smaller, reduces the number of cell adhesion ligands and causes cardiac cell death. These hydrogels present a different behavior between their liquid and solid form, in terms of their shear elastic and viscous moduli (supplementary figures 3(C)–(F)), which does not change for non-crosslinked hydrogels. This is important as cells will be bioprinted in their liquid form when extruded through the nozzle (30 °C), whereas they will be crosslinked at a lower temperature (4 °C). Nevertheless, they all gel regardless of the addition of SF at the same temperature (19 °C).

To complete our study, we tested the viability of CSs, comprising CMs, CECs and CFs, embedded in SF-containing hybrid hydrogels and incubated in cell culture medium for 28 d. The addition of SF to 4%Alg-8%Gel hydrogels affected the viability of cardiac cells within Alg–Gel hydrogels, by decreasing the number of live cells. A significant increase in toxicity ratio was only measured in hydrogels containing 2% SF (figure 7(C)). This is consistent with the reduced pore size measured by our SEM analyses (figure 2), where the reduction of pore size of hydrogels already at 14 d provides limited space for the cells to migrate and proliferate, as well as did not guarantee enough nutrient exchange for cells to survive in the 3D microenvironment.

Finally, we evaluated whether SF had any effect on CS contractile function and cell presence. Our confocal analyses of CSs stained with antibodies against CD31, cardiac troponin T and vimentin to mark CECs, CMs and CFs respectively, displayed that 1% SF does not affect the presence and distribution of cardiac cells within the spheroids. However, it was observed a reduction in spheroid size when embedded in 1% SF-containing hydrogels (figure 8(B)). This might be related to the increase in stiffness of the hydrogels, which was previously reported to control the spheroid size [43, 47]. While their size was reduced, this also led to a stronger contractile activity in terms of FS% for CSs in 1% SF hydrogels (figure 6(B)), without negatively affect their viability at 28 d (figure 7(B)). Altogether, our findings demonstrated for the first time that SF can be added to Alg–Gel hydrogels to control their mechanical properties and cardiac cell viability and function. Future studies will be required *in vivo* to determine the applicability of SF hydrogels for long-term treatment of HF beyond the current 28 d that has been demonstrated with the application of Alg–Gel hydrogels [4].

5. Conclusions

The addition of 1%SF to Alg–Gel hydrogels can be used for bioink formulations to 3D bioprint cardiac tissues. In fact, they were successfully printable using a 3D extrusion-based bioprinting system and they improved their durability over 28 d. Additionally, increasing concentrations of SF in Alg–Gel hydrogels modulated the hydrogel mechanical properties, resulting in an increase of the elastic modulus, thus in stronger 3D architectures, as well as a reduction in the pore size. This had a strong impact on the viability of CSs embedded in Alg–Gel–SF hydrogels, where only 1%SF formulations did not affect cell viability, but it improved the contractile activity.

Data availability statement

All data that support the findings of this study are included within the article (and any supplementary files).

Acknowledgments

Laura Vettori was supported by the University of Technology Sydney with the International Research Scholarship and UTS President's Scholarships. Dr Carmine Gentile was supported by a UTS Seed Funding, Heart Research Australia Grant, Perpetual IMPACT Grant, Catholic Archdiocese of Sydney Grant for Adult Stem Cell Research and a University of Sydney/Sydney Medical School Foundation Cardiothoracic Surgery Research Grant. Thomas R Cox and Elisse C Filipe were supported by a National Health and Medical Research Council (NHMRC) Ideas (2000937), Project (1140125) and Fellowship (1158590) Grant.

We would like to thank Prof Louise Cole, Dr Amy Bottomley and Veronika Valova for their assistance during imaging and analyses at the Microbial Imaging Facility and Herbert Yuan for his assistance with SEM training and analyses at the University of Technology

Sydney (UTS) and CELLINK Life Sciences for 3D bioprinter training. We would also like to thank Linda Dement for her support in imaging 3D bioprinted patches.

ORCID iDs

H A Tran https://orcid.org/0000-0001-5668-0509
I V Kabakova https://orcid.org/0000-0002-6831-9478
C Gentile https://orcid.org/0000-0002-3689-4275

References

[1] Vettori L 2020 3D bioprinting of cardiovascular tissues for in vivo and in vitro applications using hybrid hydrogels containing silk fibroin: state of the art and challenges *Current Tissue Microenvironment Reports* **1** pp 261–76
[2] Sharma P, Wang X, Ming C L C, Vettori L, Figtree G, Boyle A and Gentile C 2021 Considerations for the bioengineering of advanced cardiac in vitro models of myocardial infarction *Small* **17** e2003765
[3] Polonchuk L *et al* 2021 Towards engineering heart tissues from bioprinted cardiac spheroids *Biofabrication* **13** 045009
[4] Roche C D *et al* 2023 3D bioprinted alginate-gelatin hydrogel patches containing cardiac spheroids recover heart function in a mouse model of myocardial infarction *Bioprinting* **30** e00263
[5] Roche C D, Sharma P, Ashton A W, Jackson C, Xue M and Gentile C 2021 Printability, durability, contractility and vascular network formation in 3D bioprinted cardiac endothelial cells using alginate-gelatin hydrogels *Front. Bioeng. Biotechnol.* **9** 636257
[6] Bociaga D, Bartniak M, Grabarczyk J and Przybyszewska K 2019 Sodium alginate/gelatine hydrogels for direct bioprinting-the effect of composition selection and applied solvents on the bioink properties *Materials* **12** 2669
[7] Łabowska M B, Cierluk K, Jankowska A M, Kulbacka J, Detyna J and Michalak I 2021 A review on the adaption of alginate-gelatin hydrogels for 3D cultures and bioprinting *Materials* **14** 858
[8] Di Giuseppe M, Law N, Webb B, A. Macrae R, Liew L J, Sercombe T B, Dilley R J and Doyle B J 2018 Mechanical behaviour of alginate-gelatin hydrogels for 3D bioprinting *J. Mech. Behav. Biomed. Mater.* **79** 150–7
[9] Baptista M *et al* 2020 Silk fibroin photo-lyogels containing microchannels as a biomaterial platform for in situ tissue engineering *Biomater. Sci.* **8** 7093–105
[10] Chan A H P *et al* 2019 Altered processing enhances the efficacy of small-diameter silk fibroin vascular grafts *Sci. Rep.* **9** 17461
[11] Filipe E C *et al* 2018 Rapid endothelialization of off-the-shelf small diameter silk vascular grafts JACC *Basic Transl. Sci.* **3** 38
[12] Nazari H, Heirani-Tabasi A, Hajiabbas M, Khalili M, Shahsavari Alavijeh M, Hatamie S, Mahdavi Gorabi A, Esmaeili E and Ahmadi Tafti S H 2020 Incorporation of two-dimensional nanomaterials into silk fibroin nanofibers for cardiac tissue engineering *J. Polym. Adv. Technol.* **31** 248–59
[13] Nazari H, Heirani-Tabasi A, Hajiabbas M, Salimi Bani M, Nazari M, Pirhajati Mahabadi V, Rad I, Kehtari M, Ahmadi Tafti S H and Soleimani M 2020 Incorporation of SPION-casein core-shells into silk-fibroin nanofibers for cardiac tissue engineering *J. Cell. Biochem.* **121** 2981–93
[14] Holland C, Numata K, Rnjak-Kovacina J and Seib F P 2019 The biomedical use of silk: past, present, future *Adv. Healthcare Mater.* **8** 1800465
[15] Floren M, Migliaresi C and Motta A 2016 Processing techniques and applications of silk hydrogels in bioengineering *J. Funct. Biomater.* **7** 26
[16] Zheng H and Zuo B 2021 Functional silk fibroin hydrogels: preparation, properties and applications *J. Mater. Chem.* B **9** 1238–58
[17] Lyu Y, Liu Y, He H and Wang H 2023 Application of silk-fibroin-based hydrogels in tissue engineering *Gels* **9** 431
[18] Narayana S, Nasrine A, Gulzar Ahmed M, Sultana R, Jaswanth Gowda B H, Surya S, Almuqbil M, Asdaq S M B, Alshehri S and Arif Hussain S 2023 Potential benefits of using chitosan and silk fibroin topical hydrogel for managing wound healing and coagulation *Saudi Pharm. J.* **31** 462–71
[19] Trucco D, Sharma A, Manferdini C, Gabusi E, Petretta M, Desando G, Ricotti L, Chakraborty J, Ghosh S and Lisignoli G 2021 Modeling and fabrication of silk fibroin-gelatin-based constructs using extrusion-based Three-dimensional bioprinting *ACS Biomater. Sci. Eng.* **7** 3306–20
[20] Wang Z, Yang H and Zhu Z 2019 Study on the blends of silk fibroin and sodium alginate: hydrogen bond formation, structure and properties *Polymer* **163** 144–53
[21] Kundu B, Rajkhowa R, Kundu S C and Wang X 2013 Silk fibroin biomaterials for tissue regenerations *Adv. Drug Deliv. Rev.* **65** 457–70
[22] Mehrotra S, de Melo B A G, Hirano M, Keung W, Li R A, Mandal B B and Shin S R 2020 Nonmulberry silk based ink for fabricating mechanically robust cardiac patches and endothelialized myocardium-on-a-chip application *Adv. Funct. Mater.* **30** 1907436
[23] Kim S H *et al* 2018 Precisely printable and biocompatible silk fibroin bioink for digital light processing 3D printing *Nat. Commun.* **9** 1620
[24] Papanicolaou M *et al* 2022 Temporal profiling of the breast tumour microenvironment reveals collagen XII as a driver of metastasis *Nat. Commun.* **13** 4587
[25] Rad M A *et al* 2022 Micromechanical characterisation of 3D bioprinted neural cell models using Brillouin microspectroscopy *Bioprinting* **25** e00179
[26] Villalba-Orero M, Jiménez-Riobóo R J, Gontán N, Sanderson D, López-Olañeta M, García-Pavía P, Desco M, Lara-Pezzi E and Gómez-Gaviro M V 2021 Assessment of myocardial viscoelasticity with Brillouin spectroscopy in myocardial infarction and aortic stenosis models *Sci. Rep.* **11** 21369
[27] Guarino V *et al* Hydrogel-based platforms for the regeneration of osteochondral tissue and intervertebral disc *Polymers* 2012 **4** 1590–612
[28] Reitmaier S, Shirazi-Adl A, Bashkuev M, Wilke H-J, Gloria A and Schmidt H 2012 *In vitro* and *in silico* investigations of disc nucleus replacement *J. R. Soc. Interface* **9** 1869–79
[29] Cui X *et al* 2020 rapid photocrosslinking of silk hydrogels with high cell density and enhanced shape fidelity *Adv. Healthc. Mater.* **9** 1901667
[30] Karimi F, Lau K, Kim H N, Och Z, Lim K S, Whitelock J, Lord M and Rnjak-Kovacina J 2022 Surface biofunctionalization of silk biomaterials using dityrosine cross-linking *ACS Appl. Mater. Interfaces* **14** 31551–66
[31] Mahmodi H, Piloni A, Utama R H and Kabakova I 2021 Mechanical mapping of bioprinted hydrogel models by brillouin microscopy *Bioprinting* **23** e00151
[32] Sharma P *et al* 2022 Biofabrication of advanced in vitro 3D models to study ischaemic and doxorubicin-induced myocardial damage *Biofabrication* **14** 025003
[33] Duangpakdee A, Laomeephol C, Jindatip D, Thongnuek P, Ratanavaraporn J and Damrongsakkul S 2021 Crosslinked silk fibroin/gelatin/hyaluronan blends as scaffolds for cell-based tissue engineering *Molecules* **26** 3191
[34] Ghezzi C E, Wang L, Behlau I, Rnjak-Kovacina J, Wang S, Goldstein M H, Liu J, Marchant J K, Rosenblatt M I and Kaplan D L 2016 Degradation of silk films in multipocket

corneal stromal rabbit models *J. Appl. Biomater. Funct. Mater.* **14** e266–76
[35] Huang Y, Sun G, Lyu L, Li Y, Li D, Fan Q, Yao J and Shao J 2022 Dityrosine-inspired photocrosslinking technique for 3D printing of silk fibroin-based composite hydrogel scaffolds *Soft Matter* **18** 3705–12
[36] Rnjak-Kovacina J, Tang F, Whitelock J M and Lord M S 2016 Silk biomaterials functionalized with recombinant domain V of human perlecan modulate endothelial cell and platelet interactions for vascular applications *Colloids Surf.* B **148** 130–8
[37] Hasturk O, Jordan K E, Choi J and Kaplan D L 2020 Enzymatically crosslinked silk and silk-gelatin hydrogels with tunable gelation kinetics, mechanical properties and bioactivity for cell culture and encapsulation *Biomaterials* **232** 119720
[38] Tan X H, Liu L, Mitryashkin A, Wang Y and Goh J C H 2022 Silk fibroin as a bioink—a thematic review of functionalization strategies for bioprinting applications *ACS Biomater. Sci. Eng.* **8** 3242–70
[39] Cui X, Li J, Hartanto Y, Durham M, Tang J, Zhang H, Hooper G, Lim K and Woodfield T 2020 Advances in extrusion 3D bioprinting: a focus on multicomponent hydrogel-based bioinks *Adv. Healthcare Mater.* **9** e1901648
[40] Joshi A, Kaur T and Singh N 2022 3D bioprinted alginate-silk-based smart cell-instructive scaffolds for dual differentiation of human mesenchymal stem cells *ACS Appl. Bio. Mater.* **5** 2870–9
[41] Kadumudi F B *et al* 2021 The manufacture of unbreakable bionics via multifunctional and self-healing silk-graphene hydrogels *Adv. Mater.* **33** e2100047
[42] Wang Q, Zhang Y, Ma Y, Wang M and Pan G 2023 Nano-crosslinked dynamic hydrogels for biomedical applications *Mater. Today Bio.* **20** 100640
[43] Li Y and Kumacheva E 2018 Hydrogel microenvironments for cancer spheroid growth and drug screening *Sci. Adv.* **4** eaas8998
[44] Feng W and Wang Z 2023 Tailoring the swelling-shrinkable behavior of hydrogels for biomedical applications *Adv. Sci.* **10** e2303326
[45] Prevedel R, Diz-Muñoz A, Ruocco G and Antonacci G 2019 Brillouin microscopy: an emerging tool for mechanobiology *Nat. Methods* **16** 969–77
[46] Rioboó R J J, Gontán N, Sanderson D, Desco M and Gómez-Gaviro M V 2021 brillouin spectroscopy: from biomedical research to new generation pathology diagnosis *Int. J. Mol. Sci.* **22** 8055
[47] Taubenberger A V *et al* 2019 3D microenvironment stiffness regulates tumor spheroid growth and mechanics via p21 and ROCK *Adv. Biosyst.* **3** e1900128